

Arginylation of Myosin Heavy Chain Regulates Skeletal Muscle Strength

Anabelle S. Cornachione,^{1,4} Felipe S. Leite,^{1,4} Junling Wang,² Nicolae A. Leu,² Albert Kalganov,¹ Denys Volgin,² Xuemei Han,³ Tao Xu,³ Yu-Shu Cheng,¹ John R.R. Yates III,³ Dilson E. Rassier,¹ and Anna Kashina^{2,*}

¹Department of Kinesiology and Physical Education, Physics and Physiology, McGill University, Montreal, QC H2W 1S4, Canada

²Department of Animal Biology, University of Pennsylvania, School of Veterinary Medicine, Philadelphia, PA 19104, USA

³The Scripps Research Institute, La Jolla, CA 92037, USA

⁴Co-first author

*Correspondence: akashina@vet.upenn.edu

<http://dx.doi.org/10.1016/j.celrep.2014.06.019>

This is an open access article under the CC BY-NC-ND license (<http://creativecommons.org/licenses/by-nc-nd/3.0/>).

SUMMARY

Protein arginylation is a posttranslational modification with an emerging global role in the regulation of actin cytoskeleton. To test the role of arginylation in the skeletal muscle, we generated a mouse model with *Ate1* deletion driven by the skeletal muscle-specific creatine kinase (*Ckmm*) promoter. *Ckmm-Ate1* mice were viable and outwardly normal; however, their skeletal muscle strength was significantly reduced in comparison to controls. Mass spectrometry of isolated skeletal myofibrils showed a limited set of proteins, including myosin heavy chain, arginylated on specific sites. Atomic force microscopy measurements of contractile strength in individual myofibrils and isolated myosin filaments from these mice showed a significant reduction of contractile forces, which, in the case of myosin filaments, could be fully rescued by rearginylation with purified *Ate1*. Our results demonstrate that arginylation regulates force production in muscle and exerts a direct effect on muscle strength through arginylation of myosin.

INTRODUCTION

Posttranslational addition of Arg to proteins (arginylation) is mediated by arginyltransferase ATE1 (Balzi et al., 1990), an enzyme that is conserved in all eukaryotic species and has been recently proposed to carry global regulatory functions (Kwon et al., 2002; Saha and Kashina, 2011; Wong et al., 2007). In higher eukaryotes, ATE1 is essential for viability and has been shown to target a variety of protein substrates and affect the development and functioning of the cardiovascular system, cell migration, and neural crest-dependent morphogenesis (Karakozova et al., 2006; Kurosaka et al., 2010, 2012; Kwon et al., 2002; Saha and Kashina, 2011; Wong et al., 2007).

Recent studies from our lab identified over 100 proteins arginylated in vivo, including a prominent subset of targets related to the actin cytoskeleton (Kurosaka et al., 2012; Saha et al., 2011; Wong et al., 2007). Arginylation of nonmuscle β -actin is essential for normal cell migration and facilitates normal actin

assembly (Karakozova et al., 2006; Saha et al., 2010). Arginylation of cardiac myofibril proteins facilitates the formation and contractility of the heart muscle, and lack of arginylation leads to age-related dilated cardiomyopathy in mice (Kurosaka et al., 2012; Ribeiro et al., 2013). These results suggest that arginylation is involved in regulation in different types of actin-related structures and may constitute a general mechanism regulating the function of actin cytoskeleton in both muscle and nonmuscle cells. However, the role of arginylation in different types of muscle and the specific protein targets that drive arginylation-dependent muscle contractility are unknown.

Here, we tested the role of ATE1 in the skeletal muscle by generating a mouse model with *Ate1* knockout (KO) driven by skeletal muscle-specific creatine kinase (*Ckmm*) promoter. Such *Ckmm-Ate1* mice were viable and outwardly normal; however, their skeletal muscle strength was significantly reduced compared to the control, without any visible changes in their muscle mass or the ultrastructure of the skeletal myofibrils. Atomic force microscopy (AFM) measurements of the contractile strength in the myofibrils isolated from the soleus muscle in these mice showed a significant reduction of active contractile forces. Mass spectrometry of the isolated skeletal myofibrils showed a limited set of proteins arginylated in an intact form on specific sites, including myosin heavy chain (MHC). AFM measurements of isolated myosin filaments from *Ate1* KO mice showed similar changes as those in whole myofibrils, suggesting that reduced contractile strength in *Ate1* KO is to a large extent dependent on myosin arginylation. Moreover, this force reduction of isolated myosin filaments was fully reversible by their rearginylation using purified *Ate1*, suggesting that arginylation-dependent regulation of myosin contractile strength constitutes an on-and-off mechanism that controls the contractility of the skeletal muscle. Our results demonstrate that arginylation regulates force production in the muscle through modification of the major components of the myofibrils and exerts a direct effect on muscle strength by arginylation of the MHC.

RESULTS

Skeletal Muscle-Specific *Ate1* KO Mice Exhibit Muscle Weakness

We have previously found that *Ate1* deletion in cardiac myocytes results in severe structural and contractile defects in the heart

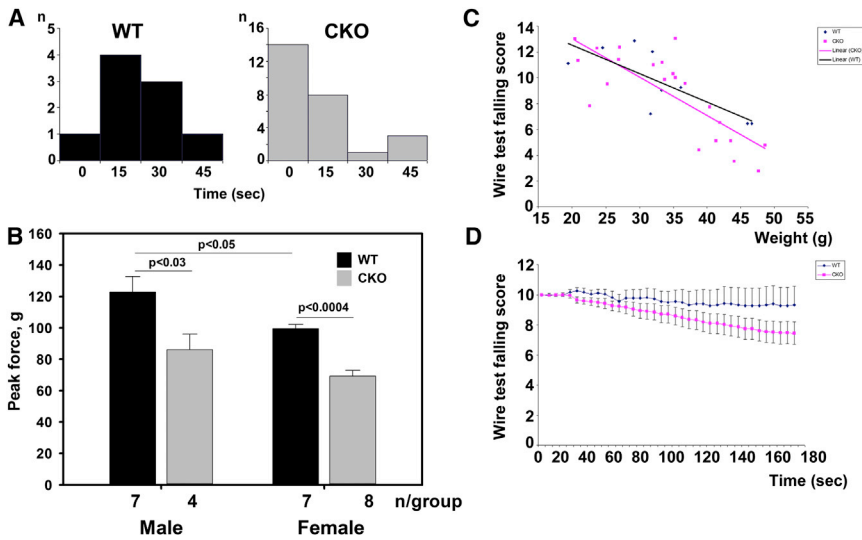


Figure 1. Ckmm-Ate1 Mice Have Reduced Skeletal Muscle Strength

(A) The duration of time WT and Ckmm-Ate1 (CKO) mice were able to hang on a horizontal wire before letting go. (B) Grip-strength measurements for males and females. (C) Wire test falling score plotted against weight in both groups. (D) Changes in wire test falling score over time in both groups. Error bars represent SEM. Measurements in all tests included 10 WT and 28 Ckmm-Ate1 mice of both sexes, approximately 6 months of age. For wire test falling scores (C and D), p value difference between the control and the Ckmm-Ate1 groups equaled 1.22×10^{-12} (determined by one-tailed paired t test). See Figure S1 for the morphology of the skeletal muscle, similar in WT and CKO mice.

muscle (Kurosaka et al., 2012; Ribeiro et al., 2013). To test whether similar effects can also be observed in the skeletal muscle, we generated a conditional skeletal muscle-specific mouse KO by crossing the previously described Ate1 floxed mice (Kurosaka et al., 2010, 2012) with the commercially available mouse line expressing Cre recombinase under the skeletal muscle-specific Ckmm promoter (Ckmm-Ate1 mice). In such mice, Cre activation occurs in skeletal myocytes upon their differentiation from myoblasts, resulting in complete deletion of Ate1 in the skeletal muscle with no expected changes in any non-muscle tissues.

Ckmm-Ate1 mice were viable, fertile, and outwardly normal and showed no obvious defects in skeletal muscle appearance or size. Ultrastructural studies of the soleus muscle from these mice also showed no marked difference from their littermate controls (Figure S1). On one occasion, a Ckmm-Ate1 mouse developed complete atrophy of the hind leg muscles, resulting in near-paralysis of the hind legs (Movie S1); however, this effect was not seen in other mice.

A prominent subset of skeletal muscle disorders leads to muscle weakness without pronounced changes in the appearance or structure of the muscle. To compare the muscular strength of Ckmm-Ate1 mice with their wild-type (WT) littermates, we performed three different tests. First, mice were tested for the duration of time they were able to spend hanging on a horizontal wire before letting go, with their hind legs bound together by a gentle restraint to prevent them from climbing onto the wire. In this test, the majority of Ckmm-Ate1 mice were able to hang on for less than 15 s, compared to the 15–30 s in the control group (Figure 1A), suggesting that these mice were overall weaker than their WT littermates. Second, grip strength was tested using a grip-strength meter (GSM), which measures the ability of a mouse to hold onto a bar when pulled away by the tail (Carbajal et al., 2009; Huang et al., 2014; Lafont et al., 2009). In this test, both male and female KO mice had 30% lower muscle strength measured as peak pull force of the forelimbs if compared to that of the WT animals (86.1 ± 9.9 g [SE] versus 122.8 ± 9.8 g, $p = 0.02$; and 69.3 ± 3.6 g versus 99.6 ± 2.6 g,

$p = 0.0003$ for males and females, respectively) (Figure 1B). Finally, mice were accessed by wire test falling score, defined as their ability to move hand over hand to the end of a horizontal wire multiple times over a 180 s time period (with a starting score of ten and each fall decreasing the score over time; Rafael et al., 2000). In this test, mutant mice showed a greater dependence of their falling score on weight, which is characteristic for mouse models with muscular dystrophy (Rafael et al., 2000) and indicates their inability to compensate for the increased weight with their muscle strength (Figure 1C). In addition, mutant mice also showed decreased ability to hold on over time, frequently letting go of the wire and receiving progressively decreasing wire test falling scores over the 180 s time period, indicating their decreased muscle strength and durability with continuous activity (Figure 1D). Overall, all these tests clearly show that Ckmm-Ate1 mice have decreased muscle strength without visible changes in any other characteristics of their skeletal muscles.

Ate1 KO Leads to Decreased Myofibril Contractile Force

To test whether the reduced muscle strength in Ckmm-Ate1 mice is directly related to the changes in intracellular contractile forces, we tested the active forces developed by individual myofibrils isolated from the soleus muscle of these mice, using AFM (Huang et al., 2014; Karakozova et al., 2006; Labuda et al., 2011). In these tests, the mutant mice exhibited significant reduction in the active contractile force (Figures 2A and 2B), which is developed by the myosin motor while interacting with actin. In order to test if the decrease in contractile force was associated with changes in the kinetics of the myosin cross bridges interacting with actin, we measured the rates of force development during initial activation (K_{act}) and after a shortening protocol (K_{tr}), as well as the rate of relaxation following deactivation (K_{rel}). All of these rates were lower in the Ckmm-Ate1 mice (Figures 2A and 2C), suggesting changes in the actomyosin kinetics cycle. SDS-PAGE analysis of the amount of MHCs in control and Ckmm-Ate1 muscles showed no significant changes in either the total levels of MHC or the myosin:actin ratio

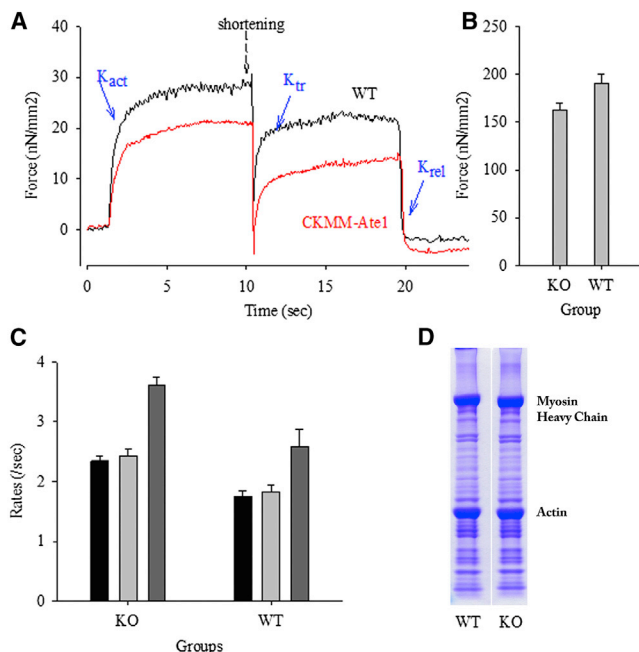


Figure 2. Atomic Force Measurements of Isolated Myofibrils Show a Decrease in Contractile Forces

(A) The active, isometric force in Ckmm-Ate1 myofibrils (KO, red) is significantly weaker than in WT myofibrils (black). After full activation was obtained, the myofibrils underwent a fast shortening protocol for measurements of force redevelopment. The rates of force development during initial activation (K_{act}), after the shortening protocol (K_{tr}), and the rate of relaxation following deactivation (K_{rel}) were obtained by exponential fits to the data. All parameters were lowered in Ckmm-Ate1 mice, suggesting changes in the actomyosin kinetics cycle.

(B) Mean values (\pm SEM) of the active forces produced by myofibrils of each group.

(C) Mean values (\pm SEM) of the K_{act} (left), K_{tr} (middle), and K_{rel} (right) produced by myofibrils of each group.

(D) Gel electrophoresis results for detection of MHC and myosin:actin ratio in a typical muscle sample from WT and Ckmm-Ate1 (KO) muscles. See also Figure S2.

(see Figure 2D for a representative gel). Thus, ATE1 appears to directly regulate active myofibril contractile force.

Several Contractile Proteins Are Prominently Arginylated in the Skeletal Myofibrils

In search for the potential mechanisms that link arginylation to the contractile strength of the skeletal muscle, we analyzed isolated skeletal myofibrils by mass spectrometry to identify which proteins are arginylated *in vivo* in these preparations. This analysis revealed a total of eight proteins, each arginylated on one or several specific sites (Table 1), including actin, MHC, myosin-binding protein C, troponin T, α -actinin, actin-capping protein, creatine kinase M, and Ub-C-terminal hydrolase 21. Arginylated sites on these proteins are located on the surface of intact proteins, within critical regions that play a role in the molecular interactions and functioning of the contractile apparatus (Figure S3). Most of these proteins constitute essential components of the contractile apparatus in the muscle, and some of them directly affect force generation during myofibril contraction (e.g., Acker-

Table 1. Proteins Arginylated in Skeletal Myofibrils

Accession Number	Name	Arginylated Site
NP_033736.1	actin, α skeletal muscle	E74
NP_038484.1	α -actinin-3	D456, D462, D465
NP_031736.1	creatine kinase M-type	D326, D335
NP_001032850.1	F-actin-capping protein subunit β isoform a	E22
NP_001034634.2	myosin heavy-chain IIa	E1169
NP_034985.2	myosin heavy-chain IIb	E887, E1005, E1012, E1166, E1500
NP_666301.2	myosin-binding protein C, fast-type isoform 2	E162
NP_001157138.1	troponin T, fast skeletal muscle isoform 4	D63
NP_001157141.1	troponin T, fast skeletal muscle isoform 5	D72
NP_038947.2	ubiquitin carboxyl terminal hydrolase 21	D439

mann and Kontrogianni-Konstantopoulos, 2011; Bais and Edwards, 1982; Bandman, 1992; Bönemann and Laing, 2004).

Myosin Arginylation Facilitates Myosin-Dependent Force Production

To dissect the likely molecular mechanism behind the reduced myofibril strength in the absence of arginylation and test the contribution of arginylation of myosin—the primary player in myofibril contractility—to the development of active contractile force, we isolated individual myosin filaments from WT and Ckmm-Ate1 mice and compared their performance while interacting with actin filaments *in vitro* using a sliding assay that can measure the velocity of actin motility, reflecting the myosin motor activity. We used commercial actin for these assays to exclude the added effect of actin arginylation. In these assays, both WT myosin and nonarginylated myosin were able to propel actin filaments with similar velocity (WT, 1.09 ± 0.17 ; KO, 1.15 ± 0.15 ; *t* test, $p = 0.29$), suggesting that the myosin motor activity was not affected by arginylation. This result is consistent with the fact that all of the arginylated sites on myosin are located in the rod region of the MHC, which mediates myosin self-association and protein-protein interactions but has no direct bearing on the activity of its motor head.

Next, we tested the force developed by the isolated myosin filaments using microfabricated cantilevers of known stiffness (Kaganov et al., 2010, 2013). In this assay, a myosin filament attached to a cantilever is brought into contact with an actin filament that is attached to another cantilever coated with α -actinin. When the filaments interact and myosin produces force, they move the actin filament, causing deflection of the cantilever proportional to the force, which reflects the strength and number of cross bridges formed between myosin and actin (see Figure S4 for a diagram of the setup). We observed that the force produced by nonarginylated myosin was significantly lower than control (Figure 3), suggesting weakened assembly of the myosin cross

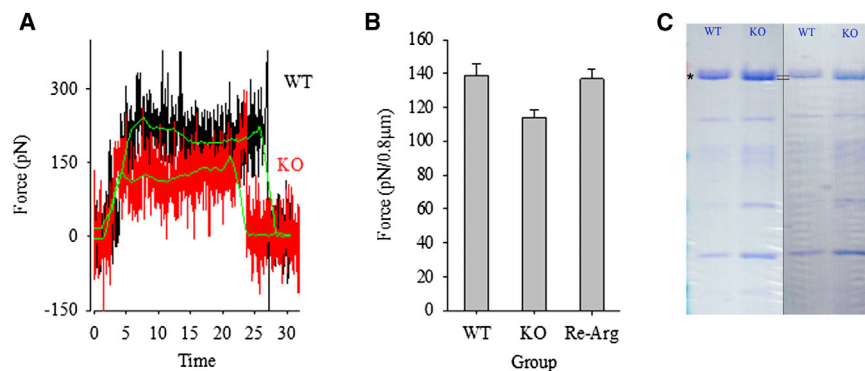


Figure 3. Arginylation of the Myosin Filaments Facilitates Myosin-Dependent Contractile Force

(A) The force produced during an interaction between actin and myosin was smaller for myosin filaments isolated from Ckmm-Ate1 muscles (KO, red) compared to WT (black).

(B) Mean values (\pm SEM) of the forces produced by three groups of myosin filaments isolated from WT, muscles, age-matched Ckmm-Ate1 muscles (KO), and Ckmm-Ate1 muscles that have been reargynated by purified Ate1 (re-Arg). Note that forces produced by myosin filaments from Ate1 KO are smaller than WT, but the force is restored by rearginylation of the filaments.

(C) SDS-PAGE of MHC (asterisk) from WT and Ckmm-Ate1 (KO) mice shows a gel shift between these two preparations (indicated by two lines on the lane interface), suggesting that the majority of MHC in WT is arginylated.

See [Figure S4](#) for the schematic representation of the measurement setup and [Figure S5](#) for a typical preparation of myosin.

bridges—the parameter that directly depends on the functionality and self-assembly properties of the myosin rod region.

To confirm that this effect was due to myosin rather than other proteins present in the myosin filament preparations, we analyzed these preparations by SDS-PAGE and mass spectrometry ([Figure S5](#)) to determine if other proteins found on our list of arginylated myofibril components shown in [Table 1](#) were present in sufficient quantities to potentially contribute to the weakened force generation. This analysis revealed that myosin constituted an overwhelming majority of the preparation. Remarkably, MHC also showed a slight gel shift into the lower molecular weight in the Ate1 KO, suggesting that the majority of this polypeptide may be arginylated in WT ([Figure 3C](#)). Among the other proteins present in the myosin filament preparation that have also been found in the arginylated protein list shown in [Table 1](#), the only detectable band on SDS-PAGE belonged to actin, which overall accounted for less than 5% of the preparation. Although the presence of minor amounts of actin might have reduced the overall efficiency of the assays, it should not have significantly affected myosin-dependent force production on externally added actin, which was present in the assays in overwhelming excess. Thus, the reduced force developed by the isolated myosin filaments from Ate1 KO muscle was due to the lack of arginylation of the MHC rather than any additional polypeptides.

To confirm that this effect was dependent on myosin arginylation and not on any other properties of the myosin filament preparations from Ate1 KO mice, we performed rescue assays, in which nonarginylated myosin filaments were reargynated in vitro by purified Ate1. The reargynated filaments were subjected to the same force assay as the control and nonarginylated filaments, using microfabricated cantilevers. Remarkably, rearginylation by Ate1 completely rescued myosin-dependent force to the control levels ([Figure 3B](#)), suggesting that reduced force developed by myosin filaments from Ckmm-Ate1 mice directly depends on arginylation.

DISCUSSION

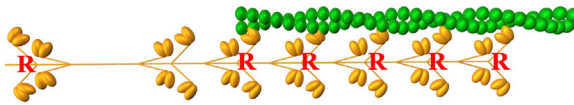
Our study demonstrates a direct effect of arginylation on force production in skeletal muscle, exerted through arginylation-

dependent regulation of the myosin motor. We have previously shown that arginylation affects cardiac myofibrillogenesis and facilitates cardiac contractility, correlated with arginylation of several myofibril proteins ([Kurosaka et al., 2012; Rai et al., 2008](#)). The present work builds on this result and demonstrates that arginylation likely plays a general role in regulating contractile strength of different types of muscles. Moreover, our finding that arginylation can directly facilitate myosin-dependent skeletal myofibril force expands the scope of the known biological effects of this emerging posttranslational modification and suggests a global regulatory mechanism for myosin in muscle contraction.

Myofibrils are the smallest structures of the skeletal muscles that still maintain the 3D lattice intact, with all major proteins present, providing a good experimental model for testing of the effect of arginylation on the muscle strength at the subcellular level. The use of this model points to several specific mechanisms that are regulated by arginylation of the myofibril proteins. The result that the specific contractile force (approximately 20% change, normalized per cross-sectional area) is decreased in Ckmm-Ate1 mice suggests that muscle weakness seen in these mice in the absence of arginylation is caused by direct structural changes in the myofibrillar contractile apparatus rather than via effects provided by other intracellular or extracellular factors.

The observed reduction in force in the absence of arginylation is similar at all sarcomere lengths investigated in this study, suggesting that this effect is independent of the initial overlap between myosin and actin filaments. Furthermore, because the decrease in force in the Ckmm-Ate1 mice is accompanied by a reduction in the rates of force development and redevelopment K_{tr} , the arginylation-dependent force decrease is likely associated with the kinetics of transition in myosin cross bridges, shifting from weakly bound to strongly bound states. Although arginylation of other proteins found in our study potentially contributes to the overall reduction in the muscle strength seen in Ckmm-Ate1 mice, the majority of these proteins are likely to contribute either to the myofibril structural integrity and the passive force that maintain the myofibril rigidity and plasticity under contraction (in the case of the structural myofibril proteins) or to the regulation of the overall muscle contractility (creatine kinase

WT: ~50% of crossbridges attached



CKO: ~30% of crossbridges attached

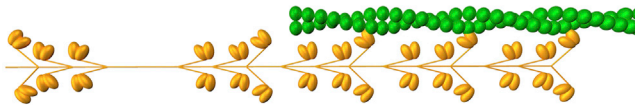


Figure 4. Arginylation of the Myosin Rod Facilitates Myosin/Actin Interaction in the Myofibril

Arginylation-induced conformational changes in the rod region of the MHC ensure the increased number of cross bridges forming between actin and myosin and facilitate cross-bridge kinetics. See also [Figure S3](#).

M) rather than exerting a direct effect on myosin-dependent contractile force. In support, the effect on the contractile force is nearly as prominent in the isolated myosin filaments as that seen in the myofibril preparations.

Myosin filaments isolated from Ckmm-Ate1 mice produce less force than control mice when normalized per filament overlap, extending the result obtained with isolated myofibrils and suggesting that the decrease in force observed in arginylation-deficient myofibrils is produced mostly at the actin-myosin interface. Because the myosin-driven sliding velocity of actin is not changed by lack of arginylation, this decrease in force is likely mediated not by a direct effect on the myosin motor activity but via the reduction of the number of myosin cross bridges attached to actin at a given time. Such reduction can be explained by the formation of filaments with fewer myosin bridges or by a slower rate of myosin attachment to actin, as suggested by our experiments with myofibrils. Both of these effects can arise from the weakened myosin self-association in the absence of arginylation within the rod of the heavy chain ([Figure S3](#)). Based on our data, we believe that the downstream effect of arginylation of the rod region on the myosin molecule results in a conformational change that facilitates the association of the myosin head with the actin filaments, resulting in normal cross-bridge kinetics ([Figure 4](#)). In the absence of arginylation, this conformational change cannot be easily achieved, and thus, the number of myosin cross bridges associated with actin at a given time is reduced. Dissecting the mechanisms of this regulation in the context of the myosin motor complex constitutes an exciting direction of further study.

Our data suggest that Ate1-mediated regulation of myofibrils exhibits commonalities in different types of muscle, including the previously characterized cardiac muscle ([Kurosaka et al., 2012](#)) and the skeletal muscle described in the present study. However, the heart muscle is apparently affected more severely by the Ate1 KO, leading to marked structural abnormalities at all developmental stages, in addition to the decreased contractile force. The lack of similar structural abnormalities in the skeletal muscle in Ckmm-Ate1 mice is likely explained by the fact that this KO occurs much later in development, thus bypassing the embryonic events that induce the early onset of skeletal myofi-

brillogenesis that generally occurs later than the formation of the cardiac muscle. It is also possible that whereas arginylation affects the contractile forces in both muscle types, it utilizes different mechanisms for regulation of skeletal and cardiac muscle. This possibility constitutes an exciting direction for further studies.

EXPERIMENTAL PROCEDURES

Mice

All the animal procedures were performed in accordance with the standards set by the University of Pennsylvania animal care and use committee. Mice with Ate1 KO in the skeletal muscle were obtained by crossing an Ate1 floxed mouse line, generated by targeted insertion of loxP sites upstream and downstream of the critical region of the Ate1 gene, with the Ckmm-Cre mouse line, commercially available from the Jackson Laboratory. After crossing, Cre recombinase expression driven by skeletal muscle-specific creatine kinase (Ckmm) promoter drives the deletion of Ate1 in skeletal muscle in the mice that are homozygous for the floxed allele and express at least one copy of the Cre transgene. These mice, termed Ckmm-Ate1, were compared with their littermate controls containing no Cre and/or no floxed allele.

Grip Strength Measurements

The forelimb muscle strength was measured using a GSM (Ugo Basile) according to the manufacturer's instructions. Following a brief habituation period, each mouse was positioned over a base plate and was allowed to grasp a bar fitted to a force transducer connected to the peak amplifier. The mouse was gently pulled back at a constant force until its grip was released. The peak pull force achieved by the animal was monitored and recorded using software supplied by the manufacturer. The test was repeated within a 30 s interval, and the results were averaged for each mouse and subjected to the statistical analysis. The significance of differences between the groups was then examined using t test. When normality criteria were not fulfilled, nonparametric analysis was performed with Mann-Whitney U test. All differences were considered significant at $p < 0.05$ (Analyse-it software).

Myofibril Preparation

Small muscle bundles of the mouse soleus muscle were dissected from WT and Ckmm-Ate1 mice, rinsed in rigor solution (50 mM Tris [pH 7.0], 100 mM NaCl, 2 mM KCl, 2 mM MgCl₂, and 10 mM EGTA), and tied to wood sticks. The samples were stored in rigor/glycerol (50:50) solution for 15 hr at -20°C and then transferred to a fresh rigor/glycerol (50:50) solution containing a cocktail of protease inhibitors (Roche Diagnostics) for at least 7 days.

Myofibril Force Measurements

On the day of the experiment, small pieces of the muscle were homogenized with rigor solution following standard procedures used in our laboratory ([Pun et al., 2010](#); [Rassier, 2008](#)). The solution with myofibrils was transferred to an experimental bath with a constant temperature of 10°C filled with a low-calcium relaxing solution ($\text{pCa}^{2+} 9.0$). Isolated myofibrils or doublets of myofibrils with 10–15 sarcomeres in series were chosen for mechanical test. Under high magnification with a $60\times$ lens (Nikon plan-fluor, NA 0.70), the myofibrils were glued to an atomic force cantilever (AFC) (model ATEC-CONTPt, Nanosensors; mean stiffness, $0.2 \text{ nN} \times \mu\text{m}^{-1}$) and a stiff glass microneedle (stiffness $>2,000 \text{ nN} \times \mu\text{m}^{-1}$). The myofibrils were lifted from the glass coverslip by approximately $150 \mu\text{m}$. With this system, a laser is shined upon and reflects from the AFC, which acts as a force transducer. The AFC deflects when an attached myofibril is shortened due to activation. The cantilever deflection is detected and recorded using a newly developed optical system that allows for high time-resolution measurements, containing an optical periscope and a photoquadrant detector. Because the stiffness of the AFCs (K) was known and we measured the amount of cantilever displacement (Δd), the force (F) could be calculated as $F = K \times \Delta d$. Before each experiment, the stiffness of AFC was confirmed using a bending method against a glass needle of known stiffness. The length and diameter of the myofibrils were measured, and the cross-sectional was calculated assuming a circular geometry.

A computer-controlled, multichannel fluidic system connected to a double-barreled pipette (Pun et al., 2010; Rassier, 2008) was used for activation/deactivation of the myofibrils (relaxing pCa^{2+} 9.0, activating pCa^{2+} 4.5). Length changes during the experiments were induced with a rigid microneedle connected to a piezo motor. Under high magnification, the contrast between the dark bands of myosin (A bands) and the light bands of actin (I bands) provided a dark-light intensity pattern, representing the striation pattern produced by the sarcomeres, which allowed measurements of sarcomere length during the experiments.

Once the myofibrils were attached to the AFCs and microneedles, they were adjusted to average sarcomere lengths between 2.2 and 3.6 μm (random order) to test the active force production at different lengths. The solution surrounding the myofibrils was changed from pCa^{2+} 9.0 to pCa^{2+} 4.5, which caused activation and force development. Once the myofibrils were fully activated and maximal force was obtained, they underwent a shortening-stretching protocol (amplitude 30% of sarcomere length; speed 10 $\mu\text{m/s}$; interval between length changes 5 ms), during which the force declined and rapidly redeveloped to reach a new steady state. The maximal force produced by the myofibrils was calculated after force development stabilization and after force redevelopment following the shortening-stretch protocol. Forces were averaged for a period of 2 s to avoid potential effects of artifacts interfering with the measured values. The passive forces produced by myofibrils during the stretching protocol were calculated when the force was stabilized at every new sarcomere length. All forces were normalized by the myofibril cross-sectional area assuming circular geometry. For each contraction, K_{act} and K_{tr} were analyzed with a two-exponential equation ($a \times (1 - \exp(-k \times t)) - \exp(-l \times t) + b$), and the K_{rel} was analyzed with a single-exponential equation ($a \times \exp(-k \times (t - c)) + b$). For both equations, "F" is force, "t" is time, "K1" and "K2" are rate constants for force development, "a" is the amplitude of the exponential(s), and "b" is the initial force value.

Biochemical Processing and MHC Electrophoresis

A total of 25 mg of frozen muscle fragments was placed in 0.5 ml solution containing 1 M Tris/HCl buffer (pH 7.4), 1 M NaCl, 0.1 M EDTA, 10% (w/v) SDS, and protease inhibitors (Roche Diagnostics). The extracts were heated at 100°C for 5 min in sample buffer containing 0.5 M Tris/HCl buffer (pH 6.8), glycerol, 10% (w/v) SDS, 0.5% (w/v) bromophenol blue, and 5% (v/v) 2-mercaptoethanol. Portions (40 μg) of each sample were analyzed by electrophoresis (SDS-PAGE 6%) using a 4% stacking gel for 2 hr at 120 V. The gels were stained with Coomassie blue. To determine the relative MHC contents, the stained gels were scanned using conventional scanner (CanoScan LiDE110; Canon).

Isolation of Native Myosin Filaments

Myosin filaments were isolated from WT and Ckmm-Ate1 mice according to standard procedures (Walker et al., 1985) with minor modifications. Briefly, muscle samples stored in rigor solution mixed with glycerol were defrosted overnight at 0°C in solution containing 140 mM NaCl, 2 mM MgCl_2 , 10 mM EGTA, 10 mM PIPES, and 2 mM DTT (pH 7.4). Muscles were diced and transferred to a cold solution containing 75 mM KCl, 2 mM MgCl_2 , 10 mM EGTA, 10 mM PIPES, 10 mM ATP, and 2 mM DTT (pH 7.0). The samples were homogenized (SNMX 1092; Omni) 2 \times for 30 s, with 1 min intervals. A total of 25 mM of KCl was added to the homogenate, and it was maintained for 2 hr at 0°C. The homogenate was centrifuged at 4,500 $\times g$ for 30 min (5804R; Eppendorf) and the supernatant diluted 4 \times in order to reduce the ionic strength and promote filament aggregation. The solution containing the filaments was kept overnight at 0°C. The next day, the solution was centrifuged at 4,500 $\times g$ for 90 min, and the pellet was resuspended in 140 mM KCl, 2 mM MgCl_2 , 2 mM EGTA, 10 mM PIPES, and 2 mM DTT (pH 7.0).

Cardiac acetone actin powder (Sigma-Aldrich) was polymerized to obtain actin filaments. The filaments were labeled using Alexa 488-phalloidin fluorescence dye (absorption/emission peaks at 488–520 nm). α -actinin (A9776; Sigma-Aldrich) was dialyzed against AB buffer 25 mM Imidazole-HCl, 25 mM KCl, 4 mM MgCl_2 , 1 mM EGTA, and 1 mM DTT.

Force Measurements in Myosin Filaments

The experimental chamber was mounted on an inverted microscope (Nikon; TE2000-U) equipped for bright-, dark-field, and/or fluorescence imaging.

Dark-field illumination was used to image myosin filaments (Labuda et al., 2011). Fluorescence microscopy was used to image actin filaments with a filter set for Alexa 488 (Exciter ET470/40 \times , Dichroic T495LP, Emitter ET525/50 m, Chroma). Images were captured with a Rolera-MGi Plus video camera (QImaging) and recorded using StreamPix4 software (NorPix; pixel size, 150 nm; rate, 30 fps).

Microfabricated cantilevers were used for measurements of force during myosin-actin interactions. The cantilevers were made out of thick silicon nitride wafer, which was followed by a photolithography process as previously used in our laboratory (Labuda et al., 2011). The cantilever tips were coated with a 50 nm gold layer in order to increase their optical contrast. The final stiffness of the cantilevers was obtained using a resonance frequency detection method as previously described by Labuda et al. (2011). The cantilevers were glued to the bottom of the metal holders, which were connected to micro-manipulators that allow 3D manipulation inside of the experimental chamber (Figure 1A).

The cantilevers attached to the metal holders were placed in the experimental chamber within a distance of \sim 10–15 mm. A total of 10 μl of myosin filament solution was added near the right cantilever, and 10 μl of α -actinin solution was added near the left cantilever, followed by a 10 min incubation period. A flow of standard AB/BSA/GOC/ATP solution (AB) (0.5 mg/ml BSA, 0.018 mg/ml catalase, 0.1 mg/ml glucose oxidase, 3 mg/ml glucose, 20 mM DTT, and 50 μM ATP) was injected into the chamber with a syringe pump (Pump 33; Harvard Apparatus) at a speed of 0.5 ml/min to wash the excess α -actinin and myosin filaments. After 2 min, the left and the right cantilevers were moved into close proximity to each other to appear in the microscope's field of view (100 \times magnification). Fluorescently labeled actin filaments (concentration, 2–4 nM) were injected into the chamber, and the flow facilitated their spontaneous attachment to the α -actinin-coated left cantilever; α -actinin is one of the major components of the Z disk in muscle sarcomeres and has high affinity for actin filaments. The flow was maintained constant to align the actin filaments approximately 90° perpendicular to the cantilevers. Myosin filaments were injected into the chamber and adhered to the right cantilever spontaneously; due to their stiffness, they did not bend with the continuous flow.

One actin filament and one myosin filament attached at or close to the cantilever tips ($<$ 50 μm from the tip) were chosen and brought closer to each other. Once the filaments interacted, they initiated force production and consequently displacement of the cantilevers, which was tracked with ImageJ software (NIH). The forces were calculated from the displacements of the cantilevers as explained previously (Kalganov et al., 2010, 2013). Briefly, the force (F) was calculated as $F = K \times \Delta d$ (cantilever displacement). The alignment of the filaments at times was not at 90° angle to the cantilever; in these cases, the force component on the vertical axis during cantilever displacement was enhanced by an angular component represented by the vertical axis. The full force generated by the filaments during interaction is therefore $F = F_x + F_y$, where "F_x" is the vector component of force along the horizontal axis, and "F_y" is the vector component of force along the vertical axis. The images of the cantilever displacements were analyzed using an automatic algorithm (ABSsnake for ImageJ; NIH).

Electron Microscopy Analysis

Soleus muscles excised from the legs of adult mice were washed in PBS and fixed in situ during excision with 2.5% glutaraldehyde and 2% paraformaldehyde in buffer C (0.1 M sodium cacodylate [pH 7.4]) followed by fixation overnight at 4°C, two 10 min washes in buffer C, and postfixation in 2% osmium tetroxide in buffer C. Muscles were washed twice for 10 min each in buffer C, once for 10 min in distilled water, incubated 1 hr at room temperature in a 2% aqueous solution of uranyl acetate, and then washed twice for 10 min each in distilled water, dehydrated by incubation for 10 min each in 50%, 70%, 80%, 90%, and 100% ethanol followed by two 5 min incubations in propylene oxide (PO), overnight incubation in 1:1 PO:Epon (Poly/Bed 812, Polysciences), and 1 day in 100% Epon. Epon-embedded samples were kept for 2 days at 60°C for Epon polymerization, sectioned, stained with 1% uranyl acetate in 50% methanol and with a 2% (w/v) solution of bismuth subnitrate at 1:50 dilution, and overlaid onto Formvar-coated grids for electron microscopy.

Mass Spectrometry

Identification of arginylated proteins by mass spectrometry was performed on isolated myofibrils as described in Wong et al. (2007) and Xu et al. (2009).

SUPPLEMENTAL INFORMATION

Supplemental Information includes Supplemental Experimental Procedures, five figures, one table, and one movie and can be found with this article online at <http://dx.doi.org/10.1016/j.celrep.2014.06.019>.

AUTHOR CONTRIBUTIONS

A.S.C., F.S.L., and J.W. designed and performed experiments. N.A.L. and A. Kalganov performed experiments. D.V. and X.H. designed and performed experiments and analyzed data. T.X. analyzed data. Y.-S.C. performed experiments. J.R.R.Y. contributed unique methods and expertise. D.E.R. contributed unique methods and expertise, designed experiments, and analyzed data. A. Kashina designed experiments, analyzed data, and wrote the paper.

ACKNOWLEDGMENTS

We thank Dr. Clara Franzini-Armstrong for help with preparations of soleus muscle for electron microscopy and for helpful suggestions throughout the project. This work was supported by the Canadian Institutes of Health Research (to D.R. and A. Kashina), NIH grants 1R01GM104003 and 1R01GM108744 (to A. Kashina), and the Pilot Grant from the Mari Lowe Center for Comparative Oncology (to A. Kashina). F.S.L. is the recipient of a CNPq scholarship, Brazil.

Received: January 26, 2014

Revised: April 2, 2014

Accepted: June 13, 2014

Published: July 10, 2014

REFERENCES

Ackermann, M.A., and Kontrogianni-Konstantopoulos, A. (2011). Myosin binding protein-C: a regulator of actomyosin interaction in striated muscle. *J. Biomed. Biotechnol.* *2011*, 636403.

Bais, R., and Edwards, J.B. (1982). Creatine kinase. *Crit. Rev. Clin. Lab. Sci.* *16*, 291–335.

Balzi, E., Choder, M., Chen, W.N., Varshavsky, A., and Goffeau, A. (1990). Cloning and functional analysis of the arginyl-tRNA-protein transferase gene ATE1 of *Saccharomyces cerevisiae*. *J. Biol. Chem.* *265*, 7464–7471.

Bandman, E. (1992). Contractile protein isoforms in muscle development. *Dev. Biol.* *154*, 273–283.

Bönnemann, C.G., and Laing, N.G. (2004). Myopathies resulting from mutations in sarcomeric proteins. *Curr. Opin. Neurol.* *17*, 529–537.

Carbajal, D., Ravelo, Y., Molina, V., Mas, R., and Arrazabala, Mde.L. (2009). D-004, a lipid extract from royal palm fruit, exhibits antidepressant effects in the forced swim test and the tail suspension test in mice. *Pharmacol. Biochem. Behav.* *92*, 465–468.

Huang, G.J., Edwards, A., Tsai, C.Y., Lee, Y.S., Peng, L., Era, T., Hirabayashi, Y., Tsai, C.Y., Nishikawa, S., Iwakura, Y., et al. (2014). Ectopic cerebellar cell migration causes maldevelopment of Purkinje cells and abnormal motor behaviour in *Cxcr4* null mice. *PLoS One* *9*, e86471.

Kalganov, A., Novinger, R., and Rassier, D.E. (2010). A technique for simultaneous measurement of force and overlap between single muscle filaments of myosin and actin. *Biochem. Biophys. Res. Commun.* *403*, 351–356.

Kalganov, A., Shalabi, N., Zitouni, N., Kachmar, L.H., Lauzon, A.M., and Rassier, D.E. (2013). Forces measured with micro-fabricated cantilevers during

actomyosin interactions produced by filaments containing different myosin isoforms and loop 1 structures. *Biochim. Biophys. Acta* *1830*, 2710–2719.

Karakozova, M., Kozak, M., Wong, C.C., Bailey, A.O., Yates, J.R., 3rd, Mogilner, A., Zebroski, H., and Kashina, A. (2006). Arginylation of beta-actin regulates actin cytoskeleton and cell motility. *Science* *313*, 192–196.

Kurosaka, S., Leu, N.A., Zhang, F., Bunte, R., Saha, S., Wang, J., Guo, C., He, W., and Kashina, A. (2010). Arginylation-dependent neural crest cell migration is essential for mouse development. *PLoS Genet.* *6*, e1000878.

Kurosaka, S., Leu, N.A., Pavlov, I., Han, X., Ribeiro, P.A., Xu, T., Bunte, R., Saha, S., Wang, J., Cornachione, A., et al. (2012). Arginylation regulates myofibrils to maintain heart function and prevent dilated cardiomyopathy. *J. Mol. Cell. Cardiol.* *53*, 333–341.

Kwon, Y.T., Kashina, A.S., Davydov, I.V., Hu, R.G., An, J.Y., Seo, J.W., Du, F., and Varshavsky, A. (2002). An essential role of N-terminal arginylation in cardiovascular development. *Science* *297*, 96–99.

Labuda, A., Brastaviceanu, T., Pavlov, I., Paul, W., and Rassier, D.E. (2011). Optical detection system for probing cantilever deflections parallel to a sample surface. *Rev. Sci. Instrum.* *82*, 013701.

Lafont, D., Adage, T., Gréco, B., and Zaratini, P. (2009). A novel role for receptor like protein tyrosine phosphatase zeta in modulation of sensorimotor responses to noxious stimuli: evidences from knockout mice studies. *Behav. Brain Res.* *201*, 29–40.

Pun, C., Syed, A., and Rassier, D.E. (2010). History-dependent properties of skeletal muscle myofibrils contracting along the ascending limb of the force-length relationship. *Proc. Biol. Sci.* *277*, 475–484.

Rafael, J.A., Nitta, Y., Peters, J., and Davies, K.E. (2000). Testing of SHIRPA, a mouse phenotypic assessment protocol, on *Dmd(mdx)* and *Dmd(mdx3cv)* dystrophin-deficient mice. *Mamm. Genome: official journal of the International Mamm. Mamm. Genome* *11*, 725–728.

Rai, R., Wong, C.C., Xu, T., Leu, N.A., Dong, D.W., Guo, C., McLaughlin, K.J., Yates, J.R., 3rd, and Kashina, A. (2008). Arginyltransferase regulates alpha cardiac actin function, myofibril formation and contractility during heart development. *Development* *135*, 3881–3889.

Rassier, D.E. (2008). Pre-power stroke cross bridges contribute to force during stretch of skeletal muscle myofibrils. *Proc. Biol. Sci.* *275*, 2577–2586.

Ribeiro, P.A., Ribeiro, J.P., Minozzo, F.C., Pavlov, I., Leu, N.A., Kurosaka, S., Kashina, A., and Rassier, D.E. (2013). Contractility of myofibrils from the heart and diaphragm muscles measured with atomic force cantilevers: effects of heart-specific deletion of arginyl-tRNA-protein transferase. *Int. J. Cardiol.* *168*, 3564–3571.

Saha, S., and Kashina, A. (2011). Posttranslational arginylation as a global biological regulator. *Dev. Biol.* *358*, 1–8.

Saha, S., Mundia, M.M., Zhang, F., Demers, R.W., Korobova, F., Svitkina, T., Perieteanu, A.A., Dawson, J.F., and Kashina, A. (2010). Arginylation regulates intracellular actin polymer level by modulating actin properties and binding of capping and severing proteins. *Mol. Biol. Cell* *21*, 1350–1361.

Saha, S., Wong, C.C., Xu, T., Namgoong, S., Zebroski, H., Yates, J.R., 3rd, and Kashina, A. (2011). Arginylation and methylation double up to regulate nuclear proteins and nuclear architecture in vivo. *Chem. Biol.* *18*, 1369–1378.

Walker, M., Knight, P., and Trinick, J. (1985). Negative staining of myosin molecules. *J. Mol. Biol.* *184*, 535–542.

Wong, C.C.L., Xu, T., Rai, R., Bailey, A.O., Yates, J.R., 3rd, Wolf, Y.I., Zebroski, H., and Kashina, A. (2007). Global analysis of posttranslational protein arginylation. *PLoS Biol.* *5*, e258.

Xu, T., Wong, C.C., Kashina, A., and Yates, J.R., 3rd. (2009). Identification of N-terminally arginylated proteins and peptides by mass spectrometry. *Nat. Protoc.* *4*, 325–332.